Measurement of Exclusive π^{0} Electroproduction Structure Functions and their Relationship to Transverse Generalized Parton Distributions

I. Bedlinskiy *et al.* (CLAS Collaboration)

Measurement of Exclusive π^0 Electroproduction Structure Functions and their Relationship to Transversity GPDs

Exclusive π^0 electroproduction at a beam energy of 5.75 GeV has been measured with the Jefferson Lab CLAS spectrometer. Differential cross sections were measured at more than 1800 kinematic values in Q^2, x_B, t, and ϕ_π, in the Q^2 range from 1.0 to 4.6 GeV^2, $-t$ up to 2 GeV^2, and x_B from 0.1 to 0.58. Structure functions $\sigma_T + \epsilon\sigma_L, \sigma_{TT}$ and σ_{LT} were extracted as functions of t for each of 17 combinations of Q^2 and x_B. The data were compared directly with two handbag-based calculations including both longitudinal and transversity GPDs. Inclusion of only longitudinal GPDs very strongly underestimates $\sigma_T + \epsilon\sigma_L$ and fails to account for σ_{TT} and σ_{LT}, while inclusion of transversity GPDs brings the calculations into substantially better agreement with the data. There is very strong sensitivity to the relative contributions of nucleon helicity flip and helicity non-flip processes. The results confirm that exclusive π^0 electroproduction offers direct experimental access to the transversity GPDs.

A major goal of hadronic physics is to describe the three dimensional structure of the nucleon in terms of its quark and gluon fields. Deep inelastic scattering experiments have provided a large body of information about quark longitudinal momentum distributions. Exclusive electron scattering experiments, in which all final state particles are measured, have been rather successfully analyzed and interpreted by Regge models which are based on hadronic degrees of freedom - for example most recently in Refs. [1, 2]. However, during the past decade the handbag mechanism has become the leading theoretical approach for extracting nucleon quark and gluon structure from exclusive reactions such as deeply virtual Compton scattering (DVCS) and deeply virtual meson electroproduction (DVMP). In this approach the quark distributions are parameterized in terms of generalized parton distributions (GPDs). The GPDs contain information about the distributions of both the longitudinal momentum and the transverse position of partons in the nucleon. In the handbag mechanism the reaction amplitude factorizes into two parts. One part describes the basic hard electroproduction process with a parton within the nucleon, and the other - the GPD- contains the distribution of partons within the nucleon which are the result of soft processes. While the former is reaction dependent, the latter is a universal property of nucleon structure common to the various exclusive reactions. This is schematically illustrated in Fig. 1. While the handbag mechanism should be most applicable at asymptotically large photon virtuality Q^2, DVCS experiments at Q^2 as low as 1.5 GeV^2 appear to be described rather well at leading twist by the handbag mechanism, while the range of validity of leading order applicability of DVMP is not as clearly determined.

There are eight GPDs. Four correspond to parton helicity conserving (chiral-even) processes, denoted by H^q, $\tilde{H}^q$, E^q and $\tilde{E}^q$. Four correspond to parton helicity-flip (chiral-odd) processes [3, 4], H_T^q, $\tilde{H}_T^q$, E_T^q and $\tilde{E}_T^q$. The GPDs depend on three kinematic variables: x, ξ and t, where x is the average parton longitudinal momentum fraction and ξ (skewness) is half of the longitudinal momentum fraction transferred to the struck parton. The skewness can be expressed in terms of the Bjorken variable x_B as $\xi \simeq x_B/(2 - x_B)$, in which $x_B = Q^2/(2p \cdot q)$, q is the four-momentum of the virtual photon and $Q^2 = -q^2$. The momentum transfer to the nucleon is $t = (p - p')^2$, where p and p' are the initial and final four momenta of the nucleon.

In the forward limit where $t \to 0$, H^q and $\tilde{H}^q$ reduce to the parton density distributions $q(x)$ and parton helicity distributions $\Delta q(x)$ respectively. The first moments in x of the chiral-even GPDs are related to the elastic form factors of the nucleon: the Dirac form factor $F_1^q(t)$, the Pauli form factor $F_2^q(t)$, the axial-vector form factor $g_A^q(t)$ and the pseudoscalar form factor $h_A^q(t)$ [5].

Most of the reactions studied, such as DVCS or vector meson production, are at leading order primarily sensitive to the chiral-even GPDs. Very little is known about the chiral-odd GPDs. H_T^q becomes the transversity function $h_1^q(x)$ in the forward limit. The chiral-odd GPDs are difficult to access since subprocesses with a quark helicity-flip are suppressed. However, a complete description of nucleon structure requires the knowledge of the transversity GPDs as well as chiral even GPDs.

Pseudoscalar meson electroproduction, and in particular π^0 production in the reaction $ep \to e'p'\pi^0$, was identified [6, 7] as especially sensitive to the helicity-flip subprocesses. Evidence of their possible contribution to π^+ electroproduction in target spin asymmetry data [8] was noted in Ref. [7]. A disadvantage of π^+ production is that the interpretation is complicated by the dominance of the longitudinal π^+-pole term, which is absent in π^0 production. In addition, for π^0 production the structure of the amplitudes further suppresses the quark helicity conserving amplitudes relative to the helicity-flip amplitudes [7]. On the other hand, π^0 cross sections over a large kinematic range are much more difficult to obtain than for π^+ for two reasons: First, the cross sections are much smaller than for π^+, and second,

the clean detection of π^0s requires the measurement of their two decay photons.

This letter presents the results of a measurement of π^0 electroproduction cross sections. The primary focus here is in its interpretation within the framework of the handbag model and on its sensitivity, within this framework, of accessing the quark helicity flip GPDs.
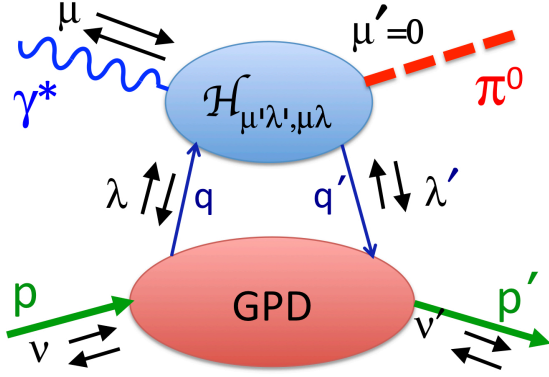

FIG. 1: Schematic diagram of the π^0 electroproduction amplitude in the framework of the handbag mechanism. The helicities of the initial and final nucleons are denoted by ν and ν', the incident photon and produced meson by μ and μ' and the active initial and final quark by λ and λ'. The arrows in the figure represent the corresponding helicities.

The handbag mechanism is schematically illustrated in Fig. 1. The reaction can be written as a linear sum of amplitudes, each of which factorizes into two processes. In the framework of Ref. [4]:

1. A process in which the incident virtual photon of helicity $\mu = 0, \pm 1$ interacts with a single quark within the nucleon having a momentum fraction $x + \xi/2$ and helicity $\lambda = \pm 1/2$, to produce a meson with helicity $\mu' = 0$ and a returning quark with momentum fraction $x - \xi/2$ and helicity $\lambda' = \pm 1/2$, which is absorbed to form the final nucleon. In the present study for transversely polarized photons $\lambda' = -\lambda$, $\mu = \pm 1$ and $\nu' = \pm \nu$.

2. Process 1 is convoluted with a GPD, which encodes the distribution of quark and gluon longitudinal momentum fractions and transverse spatial distributions within the nucleon.

The primary contributing GPDs in meson production for transverse photons are H_T, which characterizes the quark distributions involved in nucleon helicity-flip, and $\bar{E}_T (= 2\tilde{H}_T + E_T)$ which characterizes the quark distributions involved in nucleon non-helicity-flip processes [9],[10]. This GPD describes the density of transversely polarized quarks in an unpolarized nucleon [9],[10].

The relative contributions of the nucleon helicity-flip and nucleon helicity non-flip processes determine the t dependence of the differential cross sections.

Exclusive π^0 electroproduction was measured at Jefferson Lab with the CLAS large acceptance spectrometer [11]. Cross sections were extracted over a wide range in Q^2, t, x_B and ϕ_π (the azimuthal angle of the pion production plane relative to the electron scattering plane.) The incident electron beam energy was 5.75 GeV. The target was liquid hydrogen of length 2.5 cm. The integrated luminosity was 20 fb^{-1}. The CLAS detector consists of six identical sectors within a toroidal magnetic field. Each sector is equipped with three layers of drift chambers to determine the trajectory of charged particles, a gas Cherenkov counter for electron identification, a scintillation hodoscope for time-of-flight measurement, and an electromagnetic calorimeter (EC) for electron identification and photon detection for angles greater than $21°$. A forward angle calorimeter was added to the standard CLAS configuration downstream of the target for the detection of pion decay photons in the forward direction ($4.5°$ to $15°$). A superconducting solenoid around the target was used to trap Moller electrons along the beam axis, while permitting detection of photons starting at $4.5°$, protons in the range $21°$ to $60°$, and electrons from $21°$ to $45°$. All four final-state particles of the reaction $ep \rightarrow e'p'\pi^0$, $\pi^0 \rightarrow \gamma\gamma$ were detected.

The kinematic requirements for the accepted data were: $Q^2 \geq 1$ GeV^2, center-of-mass energy $W \geq 2$ GeV, and scattered electron energy $E' \geq 0.8$ GeV. The corresponding range of x_B was from 0.1 to 0.58. The electrons were identified by requiring both a Cherenkov signal and an appropriate energy deposition in the EC calorimeter. Protons were identified by TOF measurement. Geometric cuts were applied to include only regions of the detector with well understood acceptance and efficiency, as well as electron and proton target vertex position cuts, to ensure well-identified events.

The photons from $\pi^0 \rightarrow \gamma\gamma$ decays were detected in the electromagnetic calorimeters. Once all final particles were identified, the exclusive reaction $ep \rightarrow e'p'\pi^0$ was selected as follows: The angle between the direction of the reconstructed π^0s and the missing momentum for $ep \rightarrow e'p'X$ had to be less than $2°$. 3σ cuts were made on the missing mass $M_X^2(ep \rightarrow e'p'X) = m_{\pi^0}^2$, the missing mass $M_X(ep \rightarrow e'\gamma\gamma X) = M_p$, the missing energy $E_X(ep \rightarrow e'p'\pi^0) = 0$, and the invariant mass $M_{\gamma\gamma} = m_{\pi^0}$. The background under the π^0 invariant mass peak, typically 3 to 5%, was subtracted using the data in the sidebands.

Corrections for the inefficiencies in track reconstruction and detector inefficiencies were applied. The acceptance was calculated using the standard GEANT3-based CLAS Monte-Carlo simulation software. The Monte-Carlo generator for exclusive π^0 electroproduction was parameterized to be consis-

tent with the data. The ratio of the number of reconstructed Monte-Carlo events to the data events was typically a factor of about 12. Thus the statistical error introduced by the acceptance calculation was much smaller than for the data.

The data were binned in Q^2, x_B, t and ϕ_π, and differential cross sections $d^4\sigma/dQ^2 dx_B dt d\phi_\pi$ were obtained for more than 1800 bins.

Radiative corrections were calculated using the software package EXCLURAD [12], which had been previously developed and used for analyzing earlier CLAS π^0 experiments. Radiative corrections depend on Q^2, t, x_B and ϕ_π. They vary from 5 to 10%, depending on the kinematics.

An overall normalization factor of 1.12 was obtained from comparing elastic cross sections requiring e-p coincidence, with published data. A systematic uncertainty of $\pm6\%$ was applied to the resulting cross sections due to this correction.

Other systematic uncertainty studies included the electron, proton and photon particle identification, the variation of the cuts on missing masses $M_X(ep \to e'\gamma\gamma X)$ and $M_X(ep \to e'pX)$, missing energy, fiducial volumes, invariant mass $M_{\gamma\gamma}$ and radiative corrections. The overall systematic uncertainties were estimated at about 10%.

The structure functions are related to the differential cross sections by [7]

$$\frac{d^4\sigma}{dQ^2 dx_B dt d\phi_\pi} = \Gamma(Q^2, x_B, E)\frac{1}{2\pi}(\sigma_T + \epsilon\sigma_L$$
$$+\epsilon\cos 2\phi_\pi \sigma_{TT} + \sqrt{2\epsilon(1+\epsilon)}\cos\phi_\pi \sigma_{LT}). \quad (1)$$

The Hand convention [13] was adopted for the definition of the virtual photon flux factor Γ. The unseparated cross section $\sigma_U = \sigma_T + \epsilon\sigma_L$, and the interference terms σ_{LT} and σ_{TT} were extracted from the $\cos\phi_\pi$ and $\cos 2\phi_\pi$ dependences of the cross sections. The extracted structure functions as functions of $-t$ are presented in Fig. 2 for 6 of the 17 bins in Q^2 and x_B bins, for which have the largest kinematic coverage and for which there are theoretical calculations. A recent experiment, Ref. [16], measured π^0 cross sections in a limited kinematic range. When their results are projected to the present Q^2 the unseparated cross sections agree within a few percent.

The results of two GPD-based models [14, 15] are superimposed in Fig. 2. The contributions from transversely polarized photons are primarily from H_T and $\bar{E}_T$. Reference [14] obtains the following relations:

$$\sigma_T = \frac{4\pi\alpha_e}{2\kappa}\frac{\mu_\pi^2}{Q^4}[(1-\xi^2)|\langle H_T\rangle|^2 - \frac{t'}{8m^2}|\langle\bar{E}_T\rangle|^2] \quad (2)$$

and

$$\sigma_{TT} = \frac{4\pi\alpha_e}{2\kappa}\frac{\mu_\pi^2}{Q^4}\frac{t'}{8m^2}|\langle\bar{E}_T\rangle|^2. \quad (3)$$

Here $\kappa(Q^2, x_B)$ is a phase space factor, $t' = t - t_{min}$, and the brackets $\langle H_T\rangle$ and $\langle\bar{E}_T\rangle$ denote the convolution of the elementary process with the GPDs H_T and $\bar{E}_T$.

The contribution σ_L accounts for only a small fraction in both calculations (typically less than a few percent) of the unseparated $\sigma_T + \epsilon\sigma_L$ in the kinematic regime under investigation. This is because $\tilde{H}$ and $\tilde{E}$, the GPDs which are responsible for the leading-twist structure function σ_L, are very small. This is not the case for $\bar{E}_T$ and H_T which contribute to σ_T and σ_{TT}. In addition, the transverse cross sections are strongly enhanced by the chiral condensate through the parameter $\mu_\pi = m_\pi^2/(m_u + m_d)$, where m_u and m_d are current quark masses [7].

With the inclusion of the quark helicity nonconserving chiral-odd GPDs, which contribute primarily to σ_T and σ_{TT} and, to a lesser extent σ_{LT}, the model agrees moderately well with the data. Deviations in shape become greater at smaller t' for the unseparated cross section σ_U. The behavior of the cross section near the threshold t' is determined by the interplay between H_T and $\bar{E}_T$. If $\bar{E}_T$ dominates, the cross section becomes small as $t' \to 0$. For the GPDs of Ref. [14] the parameterization was guided by the lattice calculation results of Ref. [10], while Ref. [15] used a GPD Reggeized diquark-quark model to obtain the GPDs. The results in Fig. 2 for the model of Ref. [14] (solid curves), in which $\bar{E}_T$ is dominant, agree rather well with the data. In particular, the structure function σ_U begins to decrease as $-t$ becomes small, showing the effect of $\bar{E}_T$. In the model of Ref. [15] (dashed curves) H_T is dominant, which leads to a large rise in cross section as $-t'$ becomes small. Thus, in their parameterization, the relative contribution of $\bar{E}_T$ to H_T appears to be underestimated. One can make a similar conclusion from the comparison between data and model predictions for σ_{TT}. This shows the sensitivity of the measured π^0 structure functions for constraining the transversity GPDs.

From Eq. (2) for σ_T and Eq. (3) for σ_{TT} one can conclude that $|\sigma_{TT}| < \sigma_T < \sigma_U$. One sees from Fig. 2 that $-\sigma_{TT}$ is a sizable fraction of the unseparated cross section while σ_{LT} is very small, which implies that contributions from transversely polarized photons play a dominant role in the π^0 electroproduction process.

In conclusion, differential cross sections of exclusive pion electroproduction have been obtained in the few GeV region over a wide range of Q^2, x_b and t. While the general features of π^0 electroproduction have been described by recent Regge models [1, 2], the focus of this letter is on the handbag mechanism in terms of quark and gluon degrees of freedom. Within the handbag interpretation, the data appear to confirm the expectation that pseudoscalar, and
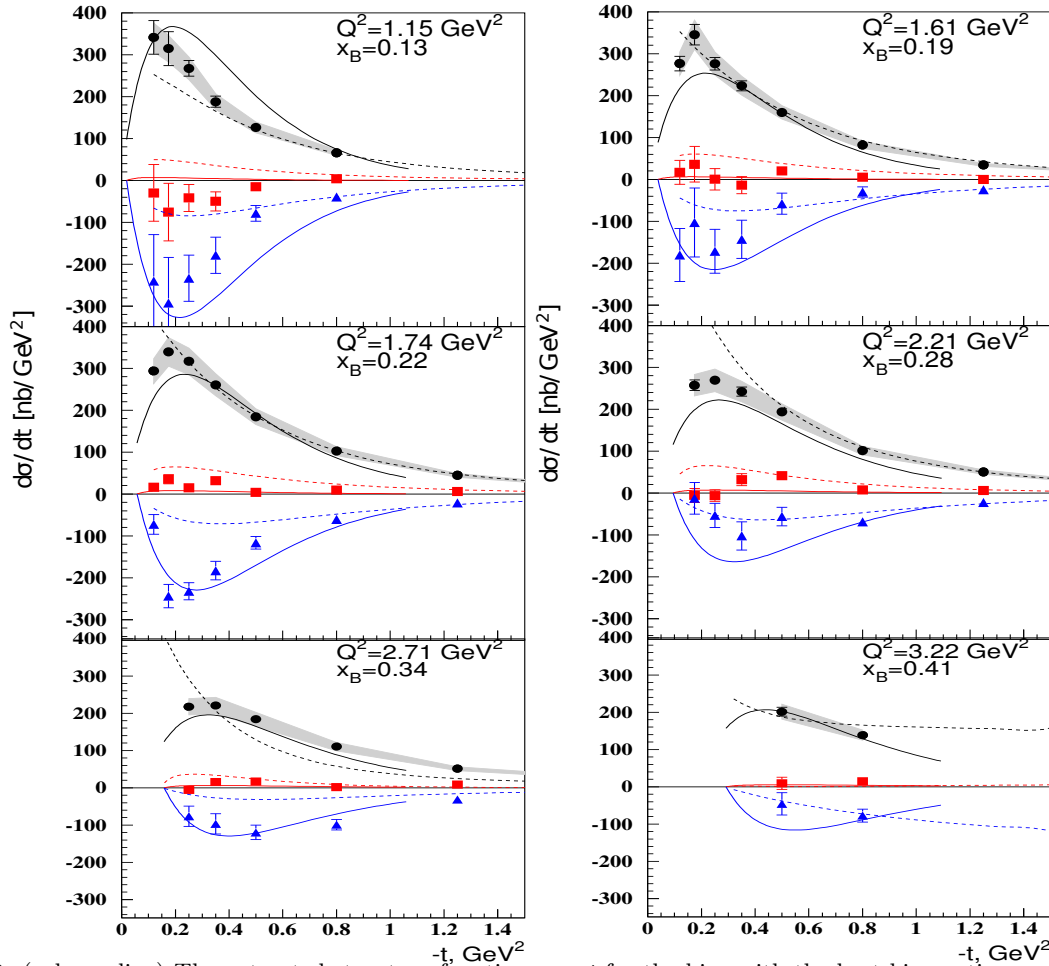
FIG. 2: (color online) The extracted structure functions vs. t for the bins with the best kinematic coverage and for which there are theoretical calculations. The solid curves are theoretical predictions produced with the models of Refs. [14] and the dashed are from [15].The data and curves are as follows: the positive value circles (black) and curves are $\sigma_U (= \sigma_T + \epsilon\sigma_L)$, the negative value triangles (blue) and curves are σ_{TT}, and the squares (red) with accompanying curves are σ_{LT}. The shaded bands reflect the experimental systematic uncertainties.

in particular π^0, electroproduction appears to be a uniquely sensitive process to access the transversity GPDs $\bar{E}_T$ and H_T. The measured unseparated cross section is much larger than expected from leading-twist handbag calculations. This means that the contribution of the longitudinal cross section σ_L is small in comparison with σ_T. The same conclusion can be made in an almost model independent way from comparison of the cross section σ_U, σ_{TT} and σ_{LT} [17].

Detailed interpretations are model dependent and quite dynamic in that they are strongly influenced by new data as they become available. In particular, calculations are in progress to compare the theoretical models with the single beam spin asymmetries obtained earlier with CLAS [18] and longitudinal target spin asymmetries which are currently under analysis.

In the near future new data on η production and ratios of η to π^0 cross sections are expected to further constrain GPD models. Extracting σ_L and σ_T with improved statistical accuracy and performing new measurements with transversely and longitudinally polarized targets would also be very useful.

————————

[1] J. M. Laget, Phys. Lett. B **695**, 199 (2011).
[2] M. M. Kaskulov, K. Gallmeister, and U. Mosel, Phys. Rev. D **78**, 114022 (2008); M. M. Kaskulov, arXiv:1105.1993.
[3] M. Diehl, Phys. Rep. **388**, 41 (2003) and references within.
[4] P. Hoodbhoy and X. Ji, Phys. Rev. D **58**, 054006 (1998).
[5] K. Goeke, M. V. Polyakov and M. Vanderhaeghen, Prog. Part. Nucl. Phys. **47**, 401 (2001).
[6] S. Ahmad, G. R. Goldstein and S. Liuti, Phys. Rev. D **79**, 054014 (2009).
[7] S.V. Goloskokov and P. Kroll, Eur. Phys. J. C **65**, 137 (2010).
[8] A. Airapetian et al. (HERMES Collaboration), Phys. Lett. B **682**, 345 (2010).
[9] M. Diehl and P. Hagler, Eur. Phys. J. C **44**, 87 (2005).
[10] M. Gockeler et al. [QCDSF Collaboration and UKQCD Collaboration], Phys. Rev. Lett. **98**, 222001 (2007).
[11] B.A. Mecking et al. Nucl. Inst. and Meth. A **503**, 513 (2003).
[12] A. Afanasev, I. Akushevich, V. Burkert and K. Joo, Phys. Rev. D **66**, 074004 (2002).
[13] L. Hand, Phys. Rev. **129**, 1834 (1963).
[14] S.V. Goloskokov and P. Kroll, Eur. Phys. J. A **47**, 112 (2011).
[15] G. R. Goldstein, J. O. Gonzalez Hernandez and S. Liuti, in preparation. G. R. Goldstein, J. O. Gonzalez Hernandez and S. Liuti, Phys. Rev. D **84**, 034007 (2011).
[16] E. Fuchey et al., Phys. Rev. C **83**, 025201 (2011).
[17] P. Kroll, private communication.
[18] R. De Masi et al., Phys. Rev. C**77**, 042201 (2008).